DOI 10.1007/s11141-018-9856-9
Radiophysics and Quantum Electronics, Vol. 60, No. 11, April, 2018
(Russian Original Vol. 60, No. 11, November, 2017)

CROSS-POLARIZATION OPTICAL COHERENCE TOMOGRAPHY WITH ACTIVE MAINTENANCE OF THE CIRCULAR POLARIZATION OF A SOUNDING WAVE IN A COMMON PATH SYSTEM

V. M. Gelikonov,[1,2] * **V. N. Romashov,**[1,2]
D. V. Shabanov,[1] **S. Yu. Ksenofontov,**[1]
D. A. Terpelov,[1] **P. A. Shilyagin,**[1,2] **G. V. Gelikonov,**[1,2]
and I. A. Vitkin[2,3]

UDC 535-4+535.012.21
+616-073.55

We consider a cross-polarization optical coherence tomography system with a common path for the sounding and reference waves and active maintenance of the circular polarization of a sounding wave. The system is based on the formation of birefringent characteristics of the total optical path, which are equivalent to a quarter-wave plate with a 45° orientation of its optical axes with respect to the linearly polarized reference wave. Conditions under which any light-polarization state can be obtained using a two-element phase controller are obtained. The dependence of the local cross-scattering coefficient of light in a model medium and biological tissue on the sounding-wave polarization state is demonstrated. The necessity of active maintenance of the circular polarization of a sounding wave in this common path system (including a flexible probe) is shown to realize uniform optimal conditions for cross-polarization studies of biological tissue.

1. INTRODUCTION

The cross-polarization optical coherence tomography (OCT) method, which is the development of the OCT, is a non-invasive interference technique allowing us to study the inner structure of biological tissue using variations in the polarization characteristics of the backscattered sounding wave [1–7]. Such variations in the backscattered-wave polarization, which are observed when compared with the specularly reflected reference wave, can be caused by several circumstances. They may involve backscattering from local optical irregularities [1, 8, 9] and the integral effects such as birefringence [10–16] and biological-tissue dichroism [17, 18]. All these effects lead to the appearance of a cross-polarization component in the backscattered radiation, whose polarization is orthogonal to that of the specularly reflected sounding wave.

The study of backscattering from local optical irregularities is of principal importance for the cross-polarization OCT method, which is mainly developed for studying soft biological tissues without birefringence (or with weak birefringence). Comparing two OCT images of biological tissue, i.e., a co-image obtained under the condition of identical polarizations of the sounding and reference waves and a cross image obtained under the condition that the reference-wave polarization changes to the orthogonal one (in the case of circular polarization of the sounding wave, rotation of the electric-field vector of the reference wave is reversed), is informative in this method. In the latter case, the reference wave interferes only with the cross component

* gelikon@ufp.appl.sci-nnov.ru

[1] Institute of Applied Physics of the Russian Academy of Sciences, [2] Nizhny Novgorod State Medical Academy, Nizhny Novgorod, Russia; [3] University of Toronto, Toronto, Canada. Translated from Izvestiya Vysshikh Uchebnykh Zavedenii, Radiofizika, Vol. 60, No. 11, pp. 1002–1018, November 2017. Original article submitted September 11, 2017; accepted November 30, 2017.

of the backscattered wave. Comparing the OCT images for the co- and cross-polarization backscattering allows one to reveal the structures deep in biological tissue, which differ by the local cross-scattering efficiency. Since the interference reception isolates only the coherent component of the backscattered radiation, the spatial resolution of the cross-polarization OCT method, as that of the conventional OCT method, has the spectrally-conditioned value that is usually equal to several microns. It should be emphasized that the cross-polarization OCT method differs from the polarization-sensitive OCT (PS OCT) method, which allows us to determine and chart the spatially-distributed optical polarization properties of biological tissue, namely, birefringence, dichroism, and orientation of its optical axes [19].

The polarization features of the coherent component of backscattered light, which are due to both cross scattering by local optical irregularities [1, 8, 9] and birefringence [10–16] or biological-tissue dichroism [17, 18], are comprehensively described by the Stokes vectors [20]. In some cases, the particular interpretation of the OCT images of individual components of the Stokes vector for the biological-tissue diagnostics contains repetitions and seems to be redundant. During the express interactive *in vivo* study of pathology of some types of biological tissue (e.g., mucosa), the simpler cross-polarization OCT method can be sufficiently informative for detecting deviations from the standard.

At present, the cross-polarization OCT method is developed in order to improve the specificity of the OCT diagnostics of biological tissues [1–4, 7, 21]. The informativeness of this method was revealed during the laboratory experiments [1, 20, 22–26] and *in vivo* biological-tissue studies [2–4, 7, 27–29] including those during *in vivo* endoscopic studies of internal organs [3, 4, 27–29] , as well as in stomatology [22, 24, 25]. The cross images of biological tissue are more "sensitive" to deviations from the standard compared with the co-polarized images. In particular, some pathologies stipulating the structural changes in biological tissue at the macro- and micro levels lead to a decrease in the intensity of the cross-polarized component of the backscattered radiation compared with the standard by a value of up to 13 dB, which can cause attenuation of these image fragments to almost the noise level [29]. In this method, obtaining the quantitative characteristics requires stable and efficient reception of the cross-polarized signal. Therefore, to improve the information reliability, one should ensure maximum-efficient reception of the cross-scattering signal and its repeatability in the cross-polarization OCT devices. However, for the linear [3, 4] or elliptic [7] polarization of the sounding wave in the cross-polarization OCT devices, the cross-image form depends on the orientation of the sample anisotropy axes with respect to the probe (in the presence of even weak birefringence properties of biological tissue) and the ellipticity degree. As was shown in the previous experiments [14, 30], the maximum efficiency of the cross-signal reception and elimination of variability of the cross-component value in the backscattered radiation can be realized using the circular-polarization radiation (the circular polarization, which is orthogonal to the reference one, has the opposite direction of the electric-field vector rotation) as a test wave. The fiber-optical cross-polarization OCT systems with a flexible probe failed to ensure the above-described optimal conditions for receiving cross-polarized radiation even when using the experience of developing the fiber systems for the polarization-sensitive OCT method [31]. This work describes the fiber-optical cross-polarization common path OCT system, which allows one to use mutually replaceable accessory, flexible probes with reproducible optical properties and is optimal for the biological-tissue sounding [7, 32]. We also describe the method of active maintenance of the circular polarization of the sounding wave in the cross-polarization common path OCT system, whose realization ensures optimal conditions and consistency of the cross-polarization measurement results.

2. MATERIALS AND METHODS

2.1. Cross-polarization backscattering dependence on the sounding-wave polarization

The lidar and radar sounding of remote objects [8, 9] employ the coefficients of the circular (δ_c) and linear (δ_l) depolarizations, which are introduced for a quantitative description of the polarization state of backscattered light. The depolarization coefficients are defined as the ratios of the intensity of the cross-polarization component to that of the co-component during incoherent reception of backscattered light with

the averaging over the entire sounding path. The cross-polarization OCT method compares the co- and cross images, which provide the two-dimensional patterns of the intensities I_{RR} and I_{RL} (I_{HH} and I_{HV}) of the interference signals detected during the cross-sectional (xz) scanning. In this case, the first and the second subscripts denote polarization of the sounding and reference waves, respectively. The subscripts R, L, H, and V denote the right-hand circular, the left-hand circular, horizontal linear, and vertical linear polarizations, respectively. The coinciding and different subscripts correspond to the co- and cross images, respectively. The co- and cross-polarization interference signals are proportional to the time- and space-averaged cross correlation of the coherent component of the sample-scattered field $\mathbf{E}_{\mathrm{R}}(t) + \mathbf{E}_{\mathrm{L}}(t)$ and the reference-wave field $\mathbf{E}_{\mathrm{R}}(t+\tau)$ (or $\mathbf{E}_{\mathrm{L}}(t+\tau)$) with the optical delay τ. The space over which the averaging is performed is bounded by the coherent-reception region at a given sounding depth and the cross-sectional size of the Gaussian beam. Variation in the scattered-signal polarization during the cross scattering can be characterized quantitatively by the ratio of the cross-correlation functions, which are proportional to the OCT signals recorded during one longitudinal scanning in the case of interference with the reference beam in the cross and co-states:

$$\delta_{\mathrm{LIN}}(z) = I_{\mathrm{HV}}(z)/I_{\mathrm{HH}}(z), \qquad \delta_{\mathrm{CIR}}(z) = I_{\mathrm{RL}}(z)/I_{\mathrm{RR}}(z). \tag{1}$$

The coefficients δ_{CIR} and δ_{LIN} can be called the cross-polarization scattering coefficients in the case of the circular and linear polarizations of the sounding wave or merely the coefficients of the circular and linear cross scattering, respectively. The similarly defined coefficient δ_{LIN} was introduced in [1] for describing the coherent component of the cross scattering for the linear polarization of the sounding wave. Note that the Stokes vectors, which are measured by the OCT method [20], as well as the coefficients δ_{CIR} and δ_{LIN}, characterize the polarization properties of only the coherent nondepolarized part of the backscattered light because of the interference reception characteristic of the OCT method.

Unlike the coefficients δ_{c} and δ_{l}, the above-introduced coefficients δ_{CIR} and δ_{LIN} characterize the ratio of the amplitudes rather than the intensities of the components of the cross- and co-polarized fields of backscattered light. In addition, these coefficients are local rather than integral characteristics over the z coordinate. When sounding short paths that are comparable with the coherence length, we have $\delta_{\mathrm{CIR}} = \sqrt{\delta_{\mathrm{C}}}$ and $\delta_{\mathrm{LIN}} = \sqrt{\delta_{\mathrm{L}}}$. For totally smooth targets and for single scattering from the spherical particles, $\delta_{\mathrm{C}} = \delta_{\mathrm{L}} = 0$ [1, 8, 9].

Some works study the cross-scattering effect in model objects. The cross-polarized backscattering is mainly observed during single scattering from nonspherical particles and multiple scattering from the particles with relatively large diameter or the clusters of particles [1, 8, 9]. The relationship between the coherent and incoherent components in the backscattered radiation significantly depends on the observation conditions, which was demonstrated in the case of scattering of the linearly polarized light in the 10% water suspension of the submicron polystyrene spheres with dimensions close to the light wavelength [33]. An increase in the intensity of the coherent component of the backscattered light by 75% and 25% compared with the incoherent component was observed for the co- and cross-polarized radiation, respectively. In both cases, the increase was localized within a narrow (about one degree) cone, which was explained by multiple scattering. According to the theoretical model, the angular dimension of the cone is determined by the ratio of the wavelength to the mean free-path length between multiple elastic collisions [33, 34]. As a result, for the coherent part of the wave, which is obtained during the scattering of a linearly polarized wave, the cross-polarization effect is described by the quantity $\delta_{\mathrm{L}} = 1/3$. According to the estimates, during the radar measurements in the case of incoherent reception, and randomly oriented dipoles, the coefficients of linear and circular depolarizations are $\delta_{\mathrm{L}} = 1/3$ and $\delta_{\mathrm{C}} = 1$, respectively [9, 35]. For all radar-detected planetary targets, we have $\delta_{\mathrm{L}} < 1$ and $\delta_{\mathrm{L}} < \delta_{\mathrm{C}}$ [8, 9].

During the cross-polarization OCT study of the coherent components of the co- and cross-polarized backscattered light in biological tissue, one can expect similar effects. In particular, during the OCT sensing, the image-developing backscattered light, in addition to the ballistic (directly flying) photons, also contains multiply scattered photons, which have the same total delay. For a short (shorter than the sounding-wave

coherence length) mean free-path length the elastic collisions, the coherent component of multiple scattering is localized in a sufficiently large cone, which can effectively overlap the angular reception pattern of an optical OCT probe (a typical numerical aperture of the probe amounts to about 0.04). The above-mentioned multiple-scattering effect leading to a variation in the relationships between the co- and cross components of coherent scattering in the case of linear polarization of the sounding wave seems to be possible in live biological tissue with its complicated microstructure. For example, it was shown in [1, 30] that the value of δ_{LIN} is between 0 and 1 in the limit of a large number of samples. As a result, variability of the ratio of intensities of the cross- and co-polarization components of a backscattered coherent wave, which is due to multiple coherent scattering, can reach 4 dB in the case of random variations in the polarization state from the circular to the linear one.

The problem of improving the polarization stability of a sounding wave is especially topical for the fiber cross-polarization OCT systems with a flexible probe used to study the biological-tissue portions of both external and internal organs. In the known OCT systems considered in this work, the polarization instability is caused by the phase perturbations randomly induced in the probe fiber and having polarization anisotropy. The sounding by a wave with the stably maintained circular polarization should improve the cross-signal level, as well as uniformity and reliability of the obtained information in the fiber-optics cross-polarization OCT systems.

2.2. Description of an optical common path scheme with active maintenance of the circular polarization of a sounding wave for the cross-polarization measurements

The described cross-polarization OCT system consists of five elements. The optical scheme of this system is shown in Fig. 1. The source of the linearly polarized broadband radiation (I) consisting of the superluminescent diode (by the SUPERLUM Ltd. company), the fiber polarizer (P) with an extinction of about 30 dB [36, 37], and the Lefevre polarization control device (PC-1) supplies a linearly polarized wave to the input of the Michelson interferometer (II). The sounding wave and the pre-delayed reference wave for the subsequent interference in the Fizeau interferometer are formed in the short and long arms of the Michelson interferometer, respectively. The long arm contains the controlled Faraday cell (the polarization-rotation angle is 45°) on whose switch-on for the time of even two-dimensional scans (B scans), the co-reception is switched over to the cross reception due to a change of the linear polarization of the reference wave for the orthogonal one. Unit (III) maintaining the circular polarization of the sounding wave, whose operation is described below, is the third element of the considered OCT system. Probe (IV) with the measuring Fizeau interferometer at the output is the fourth element. In this interferometer, the reference wave reflected from the end of the probe fiber interferes with a part of the sounding wave, which is reflected from the object. The transverse scanning by the sounding beam with respect to the object is performed due to the transverse (to the beam) motion of the fiber end (the first reflector of the Fizeau interferometer) to which the focusing lens is attached. Spectrometer (V), which is linearized with respect to the wave number and records the interference spectrum of the reference and signal waves, is the fifth element of the system [38].

The described optical system operates as follows. The linearly polarized radiation with a wavelength of 1320 nm and a spectrum width of 100 nm is supplied to both arms of the Michelson interferometer via the isotropic beam divider (50:50) from the superluminescent-diode output to form the compensating delay L_0 between the reference and sounding waves, which is equal to the delay between the backscattered and reference waves in the Fizeau interferometer. For the odd B scans for which the co-polarized images are recorded, two collinearly polarized waves are introduced to the fiber part of the scheme, which is made of SMF-28 fiber, from the Michelson-interferometer output. Then both waves are supplied to the fiber probe via the three-port circulator and the polarization controller (PC-2), as well as the system maintaining the circular polarization of the sounding wave. The optical path from the Michelson-interferometer output to the probe-fiber end and backwards to the spectrometer is common for the signal and reference waves

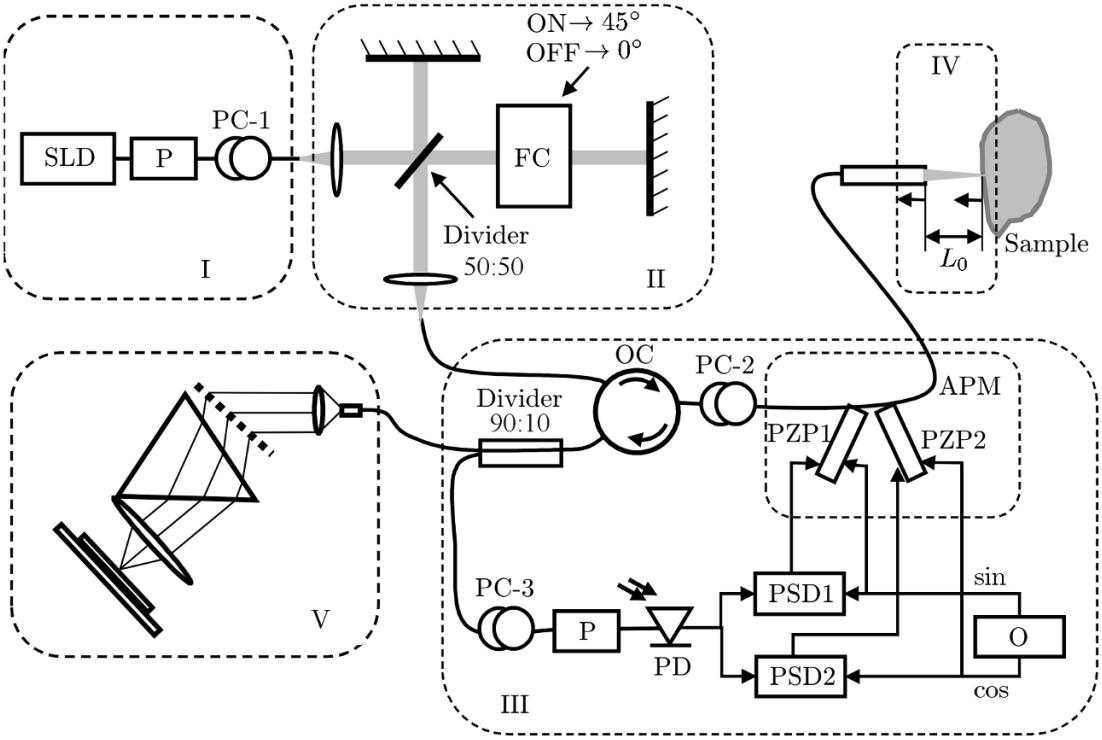

Fig. 1. Optical scheme of the described cross-polarization OCT system based on the common path principle for the signal and reference waves (common path system) with the system of automatic control of circular polarization of the sounding wave. Here, element I is the source of the linearly polarized broadband radiation, II is the compensating Michelson interferometer with the reference-wave polarization control on the basis of the Faraday cell (FC), which ensures the polarization-wave rotation to 45° during one passage when switched on, III is the system of remote control of circular polarization, which is based on two active phase modulators (APMs) of polarization, i.e., the phase plates created by the fiber compression in the transverse direction using electrically controlled piezoelectric-crystal plates PZP1 and PZP2, IV is the probe with the Fizeau interferometer, V is the spectrometer, SLD is the superluminescent diode, PC-1, PC-2, and PC-3 are the fiber polarization controllers, BS: 50-50 is the fiber coupler, OC is the optical circulator, P denotes the fiber polarizers, PD is the photodiode, O is the oscillator, and PSD 1 and PSD 2 are the phase-sensitive detectors.

according to the common path system principle [31]. The polarization controller PC-2 is used to recover the linear polarization state at the fiber output with the electric-field vector rotation to 45° with respect to the axes of the first element of the active polarization modulator (APM). The minor part of light reflected back from the fiber end in the probe is directed via the 90:10 isotropic beam divider and supplied to the photodiode of the polarization-control system via the polarizer. The remaining major part of light is supplied to the spectrometer. The system of control of the sounding-wave polarization mode is preliminary adjusted using the polarization controller (PC-30) with respect to the minimum of the light transmission through the polarizer (P) with maintained circular polarization at the probe output using manual control. In this case, the scheme segment between the Michelson-interferometer output and the polarization-modulator input becomes equivalent to the segment between the polarization-modulator output and the polarizer from the viewpoint of the phase anisotropy. As is shown below, the optical-system part, which successively includes the paths from the Michelson-interferometer output, the circulator segment 1–2, the polarization controller PC-2, the polarization modulator, the reflecting probe-fiber end (the first reflector of the Fizeau interferometer), and the return path to the polarizer via the circulator outputs 2–3, is in its operation mode equivalent to the quarter-wave plate. Alternating voltage in the system of automatic polarization control is

supplied from a common oscillator to the active elements PZP1 and PZP2 of the polarizer modulator with the quadrature phase shift by the method described in [39]. The error signals in both quadrature channels are formed by the value of the first harmonic at the output of the common photodiode which detects the light transmitted through the polarizer.

The response time of the realized automatic-control system amounts to about one tenth of a second. In this case, the circular polarization was stably maintained with the ellipticity parameter close to $\pi/4$ with accuracy up to several percent for all manipulations with the flexible probe. This allowed one to perform sounding using manual positioning of the probe during both external and endoscopic studies of biological tissue.

2.3. Method for active control of the polarization state

As is known, when linearly polarized light is supplied to the quarter-wave plate input at an angle of 45° to its optical axes, the radiation polarization at the plate output is circular. After the return passage through the plate, the light has a linear polarization which is orthogonal to the input one [40, 41]. This is the basis for the method of remote polarization control [42]. In the considered case, a part of the optical path of the polarization-control system including the polarization modulator jointly with the probe should represent a quarter-wave plate from the optical viewpoint. Consider the conditions required for realization and active maintenance of such an effective quarter-wave plate, as well as the polarization-modulator options.

The method of reaching and maintaining the required polarization properties of the fiber path depends on the chosen mechanism of the phase-delay control. In fiber optics, there exist several methods for creating electrically controlled analogs of the phase plate due to distributed action on the fiber within the limits of the optical path, which is many times longer than the wavelength [39]. To this end, radial compression of a fiber by using electromagnets was described in [43]. Using three electrically controlled polarization changers located at an angle of 45° to one another, any polarization mode was reached in the case of an arbitrary initial state [43]. However, the fiber-based control scheme is rather complicated since it requires to form and mutually adjust three control elements. There exist two-element phase optical elements with control performed by varying the angle between the anisotropy axes of the phase plates [44], as well as the birefringence control for this angle amounting to 45° [45]. Each of the above systems has some disadvantages. In this work, we consider a fiber-optics analog of the system described in [45], which also consists of two successive electrically controlled phase plates whose optical axes are oriented at an angle of 45° to each other. Since this variant is the most attractive for use in the OCT devices, it was chosen for realizing the cross-polarization OCT unit. It can be shown that an arbitrary polarization can be obtained at the output of such a two-element controller if a linearly-polarized wave with an inclination of 45° with respect to the axes of the first phase plate is maintained at its input. Therefore, the required polarization predistortions can be created at the fiber-probe input for forming circular polarization at the probe output in the case of any perturbations.

The light polarization in a fiber-optics system is well described using the Jones vectors and matrices. From the optical viewpoint, the fiber-optical path of the probe, which is based on the one-mode fiber, is a set of randomly oriented arbitrary phase plates, whose action, according to [46], is analogous to that of an equivalent phase plate with the Jones matrix $\mathbf{J}(\phi)$, which is rotated to the angle ϑ, and the rotator $\mathbf{R}(\gamma)$ and is described by the matrix $\mathbf{W}$ [47]

$$\mathbf{W} = \mathbf{R}(\gamma)\mathbf{R}(\vartheta)\mathbf{J}(\phi)\mathbf{R}(-\vartheta). \tag{2}$$

Here,

$$\mathbf{J}(\phi) = \exp(i\phi/2)\begin{pmatrix}\exp(i\phi/2) & 0;\\ 0 & \exp(-i\phi/2)\end{pmatrix}, \qquad \mathbf{R}(\alpha) = \begin{pmatrix}\cos\alpha & \sin\alpha;\\ -\sin\alpha & \cos\alpha\end{pmatrix},$$

$\phi = (2\pi/\lambda)\,(n_{\mathrm{sl}} - n_{\mathrm{f}})L$, $n_{\mathrm{sl}} - n_{\mathrm{f}}$ is the difference of the refractive indices for the slow (n_{sl}) and fast (n_{f}) axes,

L is the phase-plate thickness, and λ is the wavelength.

Polarization of the elliptically polarized quasimonochromatic wave is described using the Jones vector [48]

$$\mathbf{E} = \begin{pmatrix} E_x \\ E_y \end{pmatrix} \exp(i\omega t) = E_0 \begin{pmatrix} \cos\theta\cos\varepsilon - i\sin\theta\sin\varepsilon \\ \sin\theta\cos\varepsilon + i\cos\theta\sin\varepsilon \end{pmatrix}. \tag{3}$$

Here, E_x and E_y are the complex components of the transverse vector of the electric field of an optical wave, the angle ε is the ellipticity, θ is the azimuth of the major axis of the polarization ellipse, which is reckoned from the x axis, as the angles ϑ and γ. The Jones vectors at the system output ($\mathbf{E}_{\text{out}}$) and input ($\mathbf{E}_{\text{in}}$) are related as

$$\mathbf{E}_{\text{out}} = \mathbf{W}\mathbf{E}_{\text{in}}. \tag{4}$$

According to [48], the wave polarization is also completely described by the complex number $\chi = E_y/E_x$. By analogy with [44], in Eq. (2), the common phase multiplier, which does not influence the polarization state, can be omitted. In addition, in the case of finite circular polarization, the rotation matrix $R(\gamma)$ in Eq. (2) can also be omitted since it does not change the number $\chi_{\text{out}} = i$, which is transformed according to the law [48]

$$\chi_{\text{out}} = \frac{w_{22}\chi_{\text{in}} + w_{21}}{w_{12}\chi_{\text{in}} + w_{11}}, \tag{5}$$

where w_{kl} with $k, l = 1, 2$ are the elements of the matrix $\mathbf{W}$ describing the action of the medium.

Therefore, in this problem, the polarization evolution in the probe fiber can be described by the equation

$$\mathbf{E}_{\text{out}} = \mathbf{R}(\vartheta)\mathbf{J}(\phi)\mathbf{R}(-\vartheta)\mathbf{E}_{\text{in}}. \tag{6}$$

For illustration, the transformation described by Eq. (6) is given on the Poincaré sphere for an arbitrarily polarized wave, using its representation in the Cartesian coordinates S_1, S_2, and S_3 [48]:

$$S_1 = 1/2\cos(2\varepsilon)\cos(2\theta), \qquad S_2 = 1/2\cos(2\varepsilon)\sin(2\theta), \qquad S_3 = 1/2\sin(2\varepsilon). \tag{7}$$

The parameters θ and ε, which determine the current polarization of the wave, are obtained from the well-known relationships [48]

$$\tan(2\theta) = \frac{2\text{Re}\,\chi}{1 - |\chi|^2}, \qquad \sin(2\varepsilon) = \frac{2\text{Im}\,\chi}{1 + |\chi|^2}. \tag{8}$$

The dot $C_1 = C_1(\theta, \varepsilon)$ on the Poincaré sphere in Fig. 2 denotes the initial, arbitrarily chosen polarization, which, after transmission through an optical fiber, is transformed to the polarization C_2, performing rotational motion over the Poincaré sphere with respect to the angular vector $\mathbf{\Omega}$ oriented in the equatorial plane at the angle -2ϑ to the VH axis. The transformation is marked by dots for a stepwise variation of the angle φ.

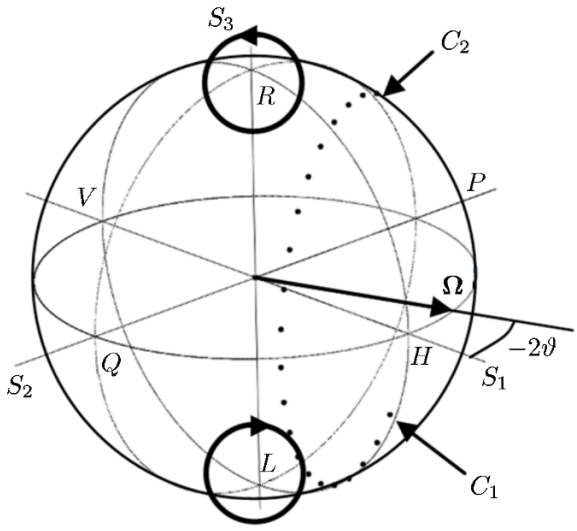

Fig. 2. The polarization-state evolution in the probe fiber in a model problem. The trajectory is given by dots.

Obviously, the sphere pole at the point R can be reached using Eq. (6) only for the "starting" polarization observed on the meridian in the plane which contains the axis RL and is normal to the angular vector $\mathbf{\Omega}$. The initial starting point on the meridian should be located at the angle φ from the pole R when rotated with respect to the vector $\mathbf{\Omega}$. Therefore, to reach circular polarization at the probe output, the active modulator of the phase anisotropy should create such a "starting" polarization in front of the probe fiber.

Let us consider conditions for the wave-polarization transformation from the linear to elliptic state with the arbitrary values of θ and ε, using active phase plates (mutual orientation of the optical axes is 45°) with the phase shifts α and β. The action of the plates is described by the matrix $\mathbf{V}$ as follows:

$$\mathbf{V}(\alpha,\beta) = \mathbf{R}(\pi/4)\mathbf{J}(\beta)\mathbf{R}(-\pi/4)\mathbf{J}(\alpha). \tag{9}$$

Here,

$$\mathbf{R}(\varphi) = \begin{pmatrix} \cos\varphi & \sin\varphi \\ -\sin\varphi & \cos\varphi \end{pmatrix}, \qquad \mathbf{J}(\beta) = \begin{pmatrix} \exp(i\beta/2) & 0 \\ 0 & -\exp(i\beta/2) \end{pmatrix}.$$

This transformation using two active phase plates, which is inverse of that studied in [45], is described by the equation

$$\exp(i\mu)\begin{pmatrix} \cos\theta\cos\varepsilon - i\sin\theta\sin\varepsilon \\ \sin\theta\cos\varepsilon + i\cos\theta\sin\varepsilon \end{pmatrix} = \mathbf{V}(\alpha,\beta)\begin{pmatrix} 1 \\ 1 \end{pmatrix}\frac{1}{\sqrt{2}} \tag{10}$$

for the initial linear polarization with the electric-field orientation at an angle of 45° to the first-controller axes:

$$\mathbf{E}_{\text{in}} = \frac{1}{\sqrt{2}}\begin{pmatrix} 1 \\ 1 \end{pmatrix}.$$

To find the desired phase shifts α and β as functions of θ and ε from Eq. (10), it is convenient to transform the left- and right-hand sides of the equation using the matrix

$$\mathbf{V}^{-1}(\alpha,\beta) = \begin{pmatrix} \cos(\beta/2)\exp(-i\alpha/2) & i\sin(\beta/2)\exp(-i\alpha/1) \\ i\sin(\beta/2)\exp(i\alpha/1) & \cos(\beta/2)\exp(i\alpha/2) \end{pmatrix}, \tag{11}$$

which is inverse with respect to the matrix $\mathbf{V}(\alpha,\beta)$. As a result, we obtain the following equation:

$$\mathbf{V}^{-1}(\alpha,\beta)\begin{bmatrix} \cos(\theta)\cos(\varepsilon) - i\sin(\theta)\sin(\varepsilon) \\ \sin(\theta)\cos(\varepsilon) + i\cos(\theta)\sin(\varepsilon) \end{bmatrix} = \exp(-i,\mu)\begin{bmatrix} 1 \\ 1 \end{bmatrix}\frac{1}{\sqrt{2}}. \tag{12}$$

On the basis of Eq. (12), for the complex number χ one can write the equations $|\chi_{\text{out}}| = 1$ and $\arg(\chi_{\text{out}}) = 0$, which yield the desired phase shifts α_0 and β_0 in the form

$$\beta_0 = \arctan\left[\frac{\cos(2\theta)}{\tan(2\varepsilon)}\right], \tag{13}$$

$$\alpha_0 = -\arctan\left[\frac{\cos(\beta_0)\tan(2\varepsilon) + \sin(\beta_0)\cos(2\theta)}{\sin(2\theta)}\right]. \tag{14}$$

Obviously, the solution of Eqs. (13) and (14) exists for any θ and $-\pi/4 \le \varepsilon \le \pi/4$, i.e., all polarization states described by the Poincare sphere are accessible. For the negative θ, the values of the phase shifts α_0 and β_0, which are obtained from Eqs. (13) and (14), correspond to the polarization transformation to the state that is normal to the state given by Eq. (4).

As an example, Fig. 3 shows that is under the action of both phase plates, the polarization transformed from the linear polarization C_1 (at an angle of 45° to the first-modulator axes) to the elliptic state C_2 with the ellipse-axis orientation 45° and then to the specified elliptic state C_3.

Let us note the necessity of the initial orientation (45° with respect to the axes of the first element of the phase modulator) of the linearly polarized wave. In the case of another orientation (such an arbitrary state is denoted by the dot C_1 in Fig. 3*b*) of the initial linear polarization at the phase-modulator input, only the states in the hatched region of the Poincaré sphere are accessible when exerting control over the two-step phase modulator. In this case, all the inaccessible regions on the Poincaré sphere can be reached only if the third active phase plate also oriented at an angle of 45° to the second plate [43] is used, which significantly complicates the structure.

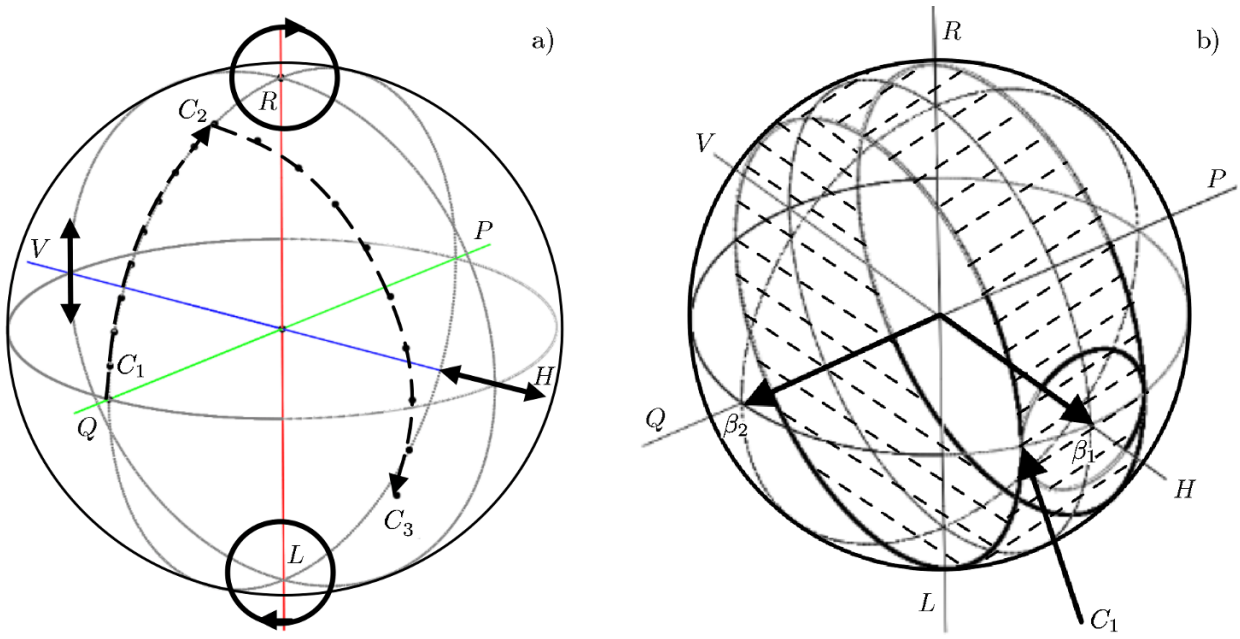

Fig. 3. The mapping polarization transformation from linear to an arbitrary one on the Poincaré sphere in cases where the inclination of the electric-field vector of the initial wave to the axes of the first element of the phase modulator is equal to 45° (*a*) and is not equal to 45° (*b*). The dashed region corresponds to the accessible resulting states).

The particular realization of the fiber-optics option of the active phase modulator was based on the mechanical compression of an optical fiber using plane piezoelectric plates. Two plate pairs oriented at an angle of 45° to each other acted on the isotropic SMF-28 fiber and realized two controlled phase shifts due to compression over the radius of the light-guiding core. By analogy with [45], only two polarization modulators with the same mutual orientation were used. Efficiency of the above-described common path system for automatic polarization control is almost not inferior to that of the system developed in [45] for an individual fiber.

3. COMPARATIVE CHARACTERISTICS OF THE SIGNALS IN THE CO- AND CROSS CHANNELS FOR CIRCULAR AND LINEAR POLARIZATIONS OF THE SOUNDING WAVE

The dependence of the signals of co- and cross scattering on the sounding-wave polarization was experimentally studied using the common path OCT device with a flexible probe (see Fig. 1). The anisotropic phase elements between the end of the distal part of the probe fiber and the object were absent, which was the necessary condition when observing the polarization characteristics of the backscattering of light. Silicon rubber with a uniform scattering structure was used as a model medium. Initially, the scanning was performed for the linear polarization of the sounding wave, which was set in the mode of manual control of the phase modulators. Then the second scanning of silicon was performed for the circular polarization of the sounding wave, which was set once the active-control system was switched on. Such operational sequence ensured minimum time between the measurements, which reduced the influence of the uncontrolled polarization variation at the fiber-probe output. In this case, all the obtained data corresponded to the same scanning place, which allowed one to perform numerical comparison.

The dependences $I_{\mathrm{HH}}(x,z)$ and $I_{\mathrm{HV}}(x,z)$ presented on the gray scale in Fig. 4*a* correspond to the backscattering signals from silicon, which are detected in the co- and cross channels, respectively, in the case of linear polarization of the sounding wave. Then the signals $I_{\mathrm{RR}}(x,z)$ and $I_{\mathrm{RL}}(x,z)$, which are shown in Fig. 4*b*, were detected for the circular polarization of the sounding wave. The images $I_{\mathrm{HH}}(x,z)$, $I_{\mathrm{HV}}(x,z)$, $I_{\mathrm{RR}}(x,z)$, and $I_{\mathrm{RL}}(x,z)$, which are presented in Figs. 4*a* and 4*b*, demonstrate a sufficiently high signal-to-

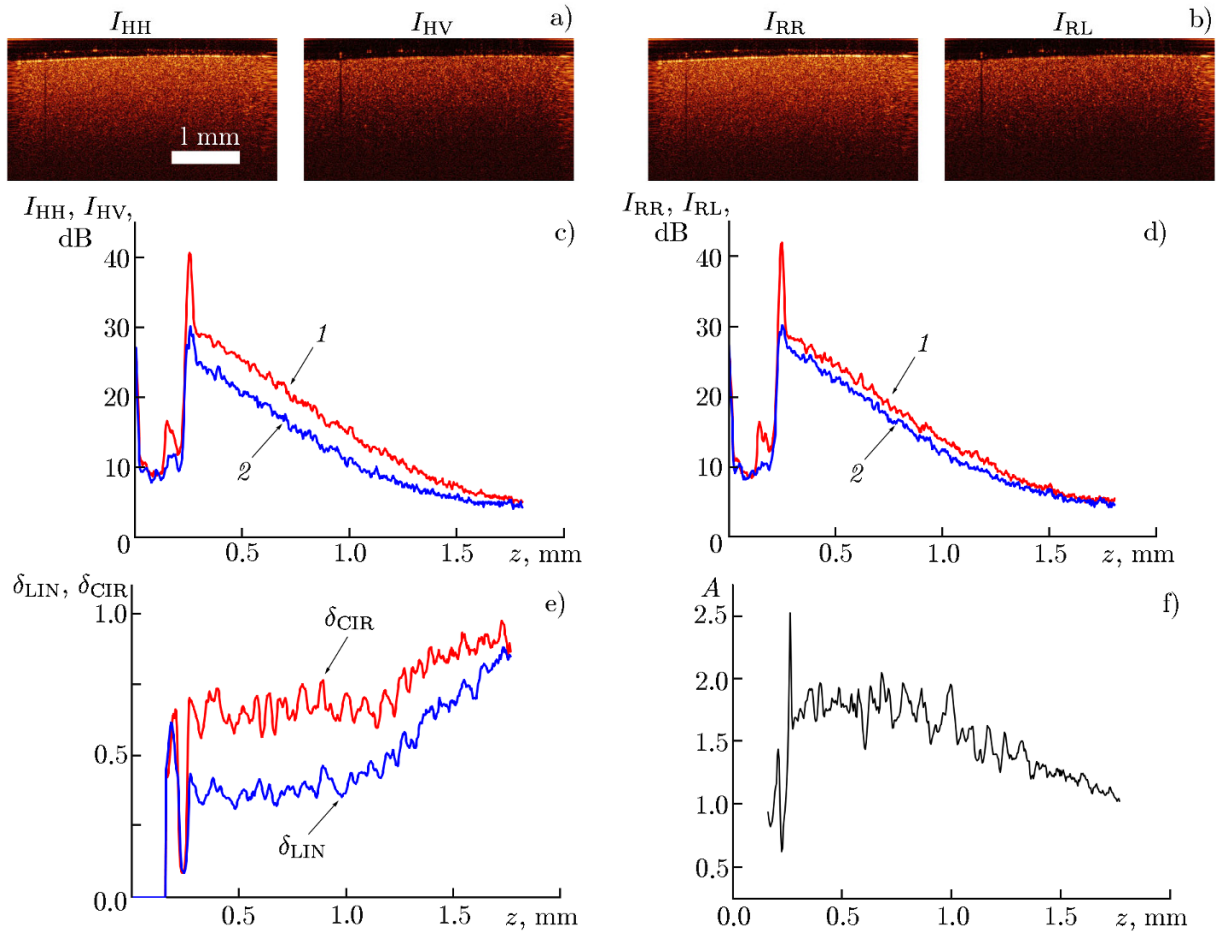

Fig. 4. Silicon-rubber scanning results: B scans $I_{HH}(x,z)$ and $I_{HV}(x,z)$ (*a*) and $I_{RR}(x,z)$ and $I_{RL}(x,z)$ (*b*), the averaged dependences $I_{HH}(z)$ (curve *1*) and $I_{HV}(z)$ (curve *2*) for a linearly polarized sounding wave (*c*) and $I_{RR}(z)$ (curve *1*) and $I_{RL}(z)$ (curve *2*) for the circular polarization of the sounding wave (*d*), and the dependences of the coefficients $\tilde{\delta}_{LIN}(z)$ and $\tilde{\delta}_{CIR}(z)$ (*e*) and their ratios $A(z) = \delta_{CIR}(z)/\delta_{LIN}(z)$ (*f*).

noise ratio, which allows one to compare the cross-scattering coefficients.

The dependences $I_{HH}(z) = \langle I_{HH}(x,z)\rangle$, $I_{HV}(z) = \langle I_{HV}(x,z)\rangle$, $I_{RR}(z) = \langle I_{RR}(x,z)\rangle$, and $I_{RL}(z) = \langle I_{RL}(x,z)\rangle$ were calculated on the basis of the four presented B scans so that each dependence was obtained using the averaging over 512 one-dimensional scans (A scans), which were reconstructed from the corresponding spectral data. In addition, the averaging was performed over the z coordinate in the interval from $z[\mu\text{m}]$ to $z[\mu\text{m}] + 20[\mu\text{m}]$ for partial smoothing of the curves. The results are given in Figs. 4*c* and 4*d* by curves *1* and *2* for the co- and cross scattering, respectively. Note that although the dependences $I_{HH}(z)$ and $I_{RR}(z)$ (co-scattering) are almost the same for the linear and circular polarizations of the sounding wave, the dependences $I_{HV}(z)$ and $I_{RL}(z)$ (cross scattering) are markedly different. Figure 4*e* shows the local cross-scattering coefficients (1) as functions of depth, calculated for the linear and circular polarizations of the sounding wave. The dependences $\delta_{LIN}(z)$ and $\delta_{CIR}(z)$ demonstrate an increase of about 3–4 dB in the cross scattering for the circular polarization compared with the cross scattering for the linear polarization for depths of about 1 mm.

The observed increase in the calculated coefficients $\delta_{LIN}(z)$ and $\delta_{CIR}(z)$ depths exceeding 1 mm is due to the influence of noise received simultaneously with the signal. Figure 4*f* shows the ratio $A(z) = \delta_{CIR}(z)/\delta_{LIN}(z)$ of the cross-scattering coefficients for the circular and linear polarizations as a function of depth. The value of $A(z)$ is about 1.6 (4 dB) from the surface to depths of about 1 mm. This value seems to be due to the effect similar to that observed during reception of the coherent component of backscattering

in the model media with spherically scattering particles sounded by the linearly polarized wave [33]. For the larger depths, the value of $A(z)$ tends to unity with increasing z, which is explained by the same noise level when receiving both the co- and cross-polarization components.

In a biological medium with complicated local structure, the dependences $\tilde{\delta}_{\mathrm{LIN}}(z)$, $\tilde{\delta}_{\mathrm{CIR}}(z)$, and $A(z)$ are obviously of another nature. Figures 5*a* and 5*b* show the images of the B scans of the chicken-leg skin for the same combinations of the sounding- and reference-wave polarizations. These images, as well as the dependences $I_{\mathrm{HH}}(z)$, $I_{\mathrm{RR}}(z)$, $I_{\mathrm{HV}}(z)$, and $I_{\mathrm{RL}}(z)$ presented in Figs. 5*c* and 5*d* and averaged over the A scans characterize the light-scattering structure of optical inhomogeneities in biological tissue, which differs from that in the model medium (silicon) and is also different for the cross scattering.

Figure 5*e* demonstrates the dependences $\delta_{\mathrm{LIN}}(z)$ and $\delta_{\mathrm{CIR}}(z)$ calculated on the basis of the obtained B scans. As was observed for silicon, the cross-scattering value is larger for the circular polarization compared with the linear one for almost all scanning depths. The function $A(z)$, which is shown in Fig. 5*f*, is calculated on the basis of these dependences. In the figures, the value of $A(z)$ is shown to exceed the unit value for depths more than 0.2 mm. The coefficient $A(z)$ reaches its maximum about 1.5 (4 dB) at a depth equal to several mean free-path lengths (about 0.6 mm). The value of $A(z)$ is close to unity both near the sample surface, where the number of cross-scattered photons is small, and at large depths at which only noise is received. Starting from the depth equal to the mean free-path length, the multiple-scattering processes also seem to play a significant role during propagation of the sounding wave in biological tissue (skin). By analogy with single scattering, a part of the multiply scattered photons presumably forms a coherent component of the backscattered wave in biological tissue. As a result, the intensity of the coherent component of cross scattering is higher for the circular polarization of the sounding wave compared with linear polarization. In our experiments, this effect, which is described in [33, 34], was more pronounced in silicon than biological tissue.

The dependences for the coefficients $A(z)$, which were calculated for three parts of the chicken-leg skin from the B scans, are presented in Fig. 6 and demonstrate different character and higher irregularity, which seems to be due to the local features of the biological-tissue structure.

The conducted experiments confirm the above-formulated assumption, i.e., conditions that are optimal for the cross-polarization measurements are fulfilled for realization of the cross-polarization OCT method based on the common path optical scheme, provided that the circular polarization of the sounding wave is effectively maintained. In this case, the uncertainty of the cross-scattering value, which could be caused by a variation in the sounding-wave polarization during the fiber bends, is eliminated. As was discussed above, this uncertainty can reach 4 dB due to the multiple coherent-scattering effect, which has a peculiarity during linear polarization of the wave. It is also evident that the image contrast is increased during the cross-polarization scattering at the medium sounding depths.

4. BIREFRINGENCE INFLUENCE DURING THE MEASUREMENTS USING THE CROSS-POLARIZATION OCT METHOD

The birefringence influence in biological tissue can be observed during the cross-polarization studies of the cutaneous covering, as well as the upper connective-tissue layers of mucosa, for which the difference between the co- and cross signals is mainly due to the local-scattering processes. This effect causes the signal modulation in the limits of the A scans, which can look as the appearance of additional (false) layers in the images. The modulation depth is maximum for the circular polarization of the sounding wave, and depends on the ellipse-axis orientation in the plane that is orthogonal to the sounding beam.

For weak birefringence of biological tissue when the signal-modulation period is comparable with the scanning depth, this modulation in both conventional OCT images and the cross-polarization ones can be unrevealed as a result of birefringence and assumed to be one of the biological-tissue layers. Such a false modulation can be revealed for the linearly polarized sounding radiation since the modulation depth depends on the sample orientation with respect to the sounding-wave polarization plane. For the circular polarization of the sounding wave, the birefringence-caused modulation can be revealed by comparing the

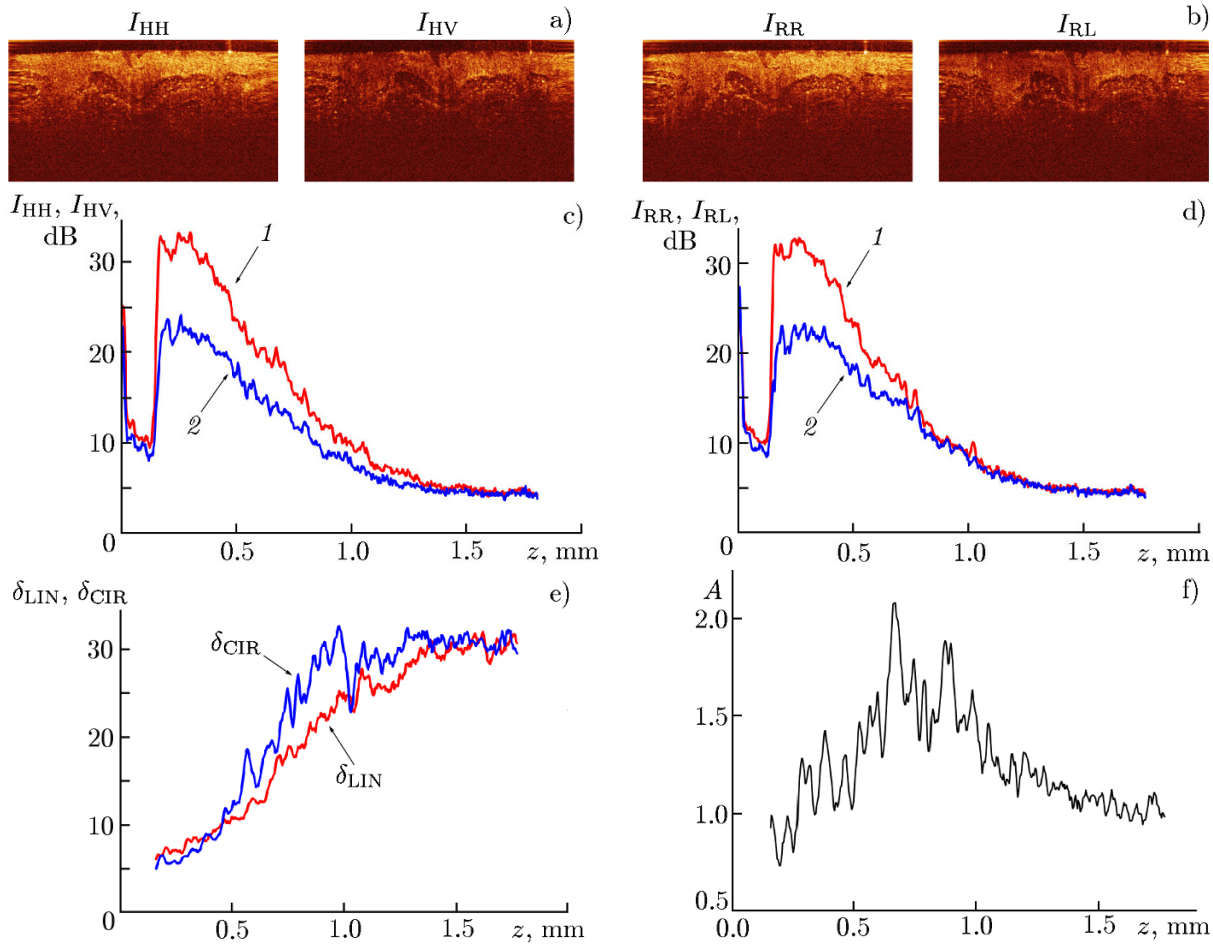

Fig. 5. The results of scanning of the chicken-leg skin: B scans $I_{HH}(x,z)$ and $I_{HV}(x,z)$ (*a*) and $I_{RR}(x,z)$ and $I_{RL}(x,z)$ (*b*), the averaged dependences $I_{HH}(z)$ and $I_{HV}(z)$ for the linearly polarized sounding wave (*c*) and $I_{RR}(z)$ and $I_{RL}(z)$ for the circular polarization of the sounding wave (*d*), and the dependences $\delta_{LIN}(z)$ and $\tilde{\delta}_{CIR}(z)$ (*e*) and their ratios $A(z) = \tilde{\delta}_{CIR}(z)/\tilde{\delta}_{LIN}(z)$ (*f*). The same notations of the curves as in Fig. 4.

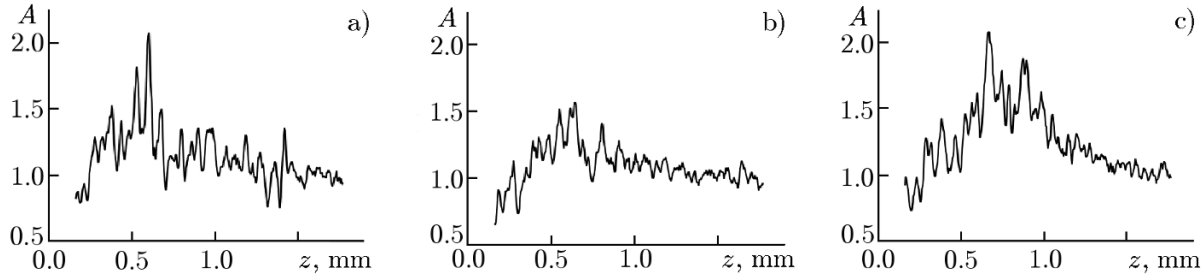

Fig. 6. The dependences of the coefficient $A(z)$ for three chicken-skin parts.

modulation laws in the co- and cross channels of the signal reception.

The strong manifestation of this effect is shown in Fig. 7 by the A scans of the co- and cross backscattering, which are averaged in the limits of the B scan, during the sounding of the chicken-leg tendon by a circularly polarized wave. Curve *4* in Fig. 7 corresponds to the dependence $I(z) = \sqrt{I^2_{CO}(z) + I^2_{CROSS}(z)}$, which is almost unaffected by the biological-tissue birefringence. The absence of the birefringence-induced modulation in the signal is indicative of realizing the same sensitivity in the co- and cross channels in the created system, as well as the presence of a quadrature (or close to quadrature) phase shift in the amplitude

modulation of signals in these channels. The possibility of eliminating the birefringence-induced modulation in the OCT images is discussed in [11] for the case of two orthogonal reception channels. Such a calculation allows one to determine the light-scattering parameters in biological tissue even under the conditions of the strong birefringence in the latter.

5. CONCLUSIONS

We have considered the cross-polarization common path OCT system with active maintenance of circular polarization of the sounding wave. The system is based on the formation of birefringence characteristics of the total optical path, which are equivalent to the quarter-wave plate with 45° orientation. The conditions have been found under which any light-polarization state can be obtained for the initially linearly polarized wave with 45° orientation with respect to the optical axes of the first element of the phase control device consisting of two active phase plates which are oriented at an angle of 45° with respect to each other. The efficiency of the system of remote automatic control of circular polarization at the fiber-interferometer output in a flexible fiber-optics probe has been demonstrated under the condition of direct and backward light transmission through the complete optical path. The dependence of the cross-polarization scattering coefficient on the sounding-wave polarization has been demonstrated by several examples. It has been shown that in the depth range equal to several free-path lengths, the local coefficient of the cross-polarization scattering is greater for the circular polarization than for the linear one and independent of the sample orientation. We have shown the necessity of maintaining circular polarization of the sounding wave in the cross-polarization OCT system since this eliminates uncertainty of the signal value in a cross channel, which can reach 4 dB without control of the sounding-wave polarization state. Observation of the signal-amplitude modulation in the orthogonal channels with mutual depth shift has been shown to allow one to identify the artifacts in the images in the form of the false biological-tissue layers due to the birefringence of the medium.

A possibility of obtaining the complete-scattering signal has been demonstrated when using the cross-polarization common path OCT system in the presence of the signal-amplitude modulation, which is induced by the birefringence of the medium, in the orthogonal channels with the quadrature shift. It should be noted that once the noise influence is suppressed (e.g., due to the averaging), the coefficients $\tilde{\delta}_{\mathrm{LIN}}(z)$ and $\tilde{\delta}_{\mathrm{CIR}}(z)$, as well as their ratio $A(z)$ can be used as informative parameters when searching for pathologic zones and as indicators of the characteristic two- and three-dimensional structures in the case of various pathologies.

The developed cross-polarization common path OCT scheme with control over the circular polarization of the sounding wave can serve as the basis for the clinical-use devices ensuring the *in vivo* sounding of both external and internal organs using sterilizable accessory probes [49].

This work was supported by the Ministry of Education and Science of the Russian Federation (contract No. 14.B25.31.0015).

REFERENCES

1. J. M. Schmitt and S. H. Xiang, *Opt. Lett.*, **23**, No. 13, 1060 (1998).
2. F. Feldchtein, V. Gelikonov, R. Iksanov, et al., *Opt. Express*, **3**, No. 6, 239 (1998).
3. R. V. Kuranov, V. V. Sapozhnikova, I. V. Turchin, et al., *Opt. Express*, **10**, No. 15, 707 (2002).
4. R. V. Kuranov, V. V. Sapozhnikova, N. M. Shakhova, et al., *Quantum Electron.*, **32**, No. 11, 993 (2002).
5. V. Sankaran, J. T. Walsh, and D. J. Maitland, *J. Biomed. Opt.*, **7**, No. 3, 300 (2002).
6. D. Fried, J. Xie, S. Shafi, et al., *J. Biomed. Opt.*, **7**, No. 4, 618 (2002).
7. V. M. Gelikonov and G. V. Gelikonov, *Laser Phys. Lett.*, **3**, No. 9, 445 (2006).
8. M. I. Mishchenko and J. W. Hovenier, *Opt. Lett.*, **20**, No. 12, 1356 (1995).
9. S. J. Ostro, *Rev. Mod. Phys.*, **65**, No. 4, 1235 (1993).

10. M. R. Hee, D. Huang, E. A. Swanson, et al., *J. Opt. Soc. Am.*, **9**, No. 6, 903 (1992).
11. J. F. De Boer, T. E. Milner, M. J. C. Van Gemert, et al., *Opt. Lett.*, **22**, No. 12, 934 (1997).
12. J. F. De Boer, S. M. Srinivas, A. Malekafzali, et al., *Opt. Express*, **3**, No. 6, 212 (1998).
13. M. J. Everett, K. Schoenenberger, B. W. Colston, Jr., et al., *Opt. Lett.*, **23**, No. 3, 228 (1998).
14. J. F. De Boer, T. E. Milner, and J. S. Nelson, *Opt. Lett.*, **24**, No. 5, 300 (1999).
15. G. Yao and L. V. Wang, *Opt. Lett.*, **24**, No. 8, 537 (1999).
16. C. K. Hitzenberger, E. Gotzinger, M. Sticker, et al., *Opt. Express*, **9**, No. 13, 780 (2001).
17. M. Todorović, S. Jiao, L. V. Wang, et al., *Opt. Lett.*, **29**, No. 20, 2402 (2004).
18. W. Drexler and J. G. Fujimoto, eds., *Optical Coherence Tomography: Technology and Applications*, Springer, Berlin (2008).
19. B. Baumann, *Appl. Sci.*, **7**, No. 5, 474 (2017).
20. S. Jiao, G. Yao, and L. V. Wang, *Appl. Opt.*, **39**, No. 34, 6318 (2000).
21. V. Yu. Zaitsev, V. M. Gelikonov, L. A. Matveev, et. al., *Radiophys. Quantum Electron.*, **57**, No. 1, 52 (2014).
22. H. Kang, J. J. Jiao, C. Lee, et al., *IEEE J. Selected Topics Quantum Electron.*, **16**, No. 4, 870 (2010).
23. C. Lammeier, Y. P. Li, S. Lunos, et al., *J. Biomed. Opt.*, **17**, No. 10, 106002 (2012).
24. R. Chen, J. Rudney, C. Aparicio, et al., *Lett. Appl. Microbiol.*, **54**, No. 6, 537 (2012).
25. K. H. Chan, A. C. Chan, W. A. Fried, et al., *J. Biophoton.*, **8**, Nos. 1–2, 36 (2015).
26. P. Lentona, J. Rudneyb, R. Chenb, et al., *Dent. Mater.*, **28**, No. 7, 792 (2012).
27. N. Gladkova, O. Streltsova, E. Zagaynova, et al., *J. Biophoton.*, **4**, Nos. 7–8, 519 (2011).
28. N. Gladkova, E. Kiseleva, N. Robakidze, et al., *J. Biophoton.*, **6**, No. 4, 321 (2013).
29. E. Kiseleva, M. Kirillin, F. Feldchtein, et al., *Biomed. Opt. Express*, **6**, No. 4, 1464 (2015).
30. V. M. Gelikonov and G. V. Gelikonov, *Quantum Electron.*, **38**, No. 7, 634 (2008).
31. K. H. Kim, B. H. Park, Y. Tu, et al., *Opt. Express*, **19**, No. 2, 552 (2011).
32. F. Feldchtein, J. Bush, G. Gelikonov, et al., *Proc. SPIE.*, **5690**, 349 (2005).
33. P. E. Wolf and G. Maret, *Phys. Rev. Lett.*, **55**, No. 24, 2696 (1985).
34. V. P. Tishkovets and M. I. Mishchenko, *J. Quant. Spectrosc. Rad. Transf.*, **110**, Nos. 1–2, 139 (2009).
35. M. W. Long, *Trans. IEEE AP-14*, **13**, No. 5, 749 (1965).
36. V. M. Gelikonov, D. D. Gusovskii, Yu. N. Konoplev, et al., *Quantum Electron.*, **17**, No. 1, 87 (1990).
37. V. M. Gelikonov, Yu. N. Konoplev, M. N. Kucheva, et al., *Opt. Spectrosc.*, **71**, No. 4, 397 (1991).
38. V. M. Gelikonov, G. V. Gelikonov, and P. A. Shilyagin, *Opt. Spectrosc.*, **106**, No. 3, 459 (2009).
39. F. A. Mohr and U. Scholz, in: S. Ezekiel and N. J. Arditty, eds., *Fiber-Optic Rotation Sensor and Related Technologies*, Springer-Verlag, Berlin–Heidelberg (1982), p. 163.
40. K. Goto, T. Sueta, and T. Makimoto, *IEEE J. Quantum Electron.*, **QE-8**, No. 6, 486 (1972).
41. H. Kuwahara, *Appl. Opt.*, **19**, No. 2, 319 (1980).
42. N. Vansteenkiste, P. Vignolo, and A. Aspect, *J. Opt. Soc. Am. A*, **10**, No. 10, 2240 (1993).
43. M. Johnson, *Appl. Opt.*, **18**, No. 9, 1288 (1979).
44. I. V. Goltser, M. Y. Darscht, N. D. Kundikova, et al., *Opt. Commun.*, **97**, Nos. 5–6, 291 (1993).

45. Y. Kidon, Y. Suematsu, and K. Furuya, *IEEE J. Quantum Electron.*, **QE-17**, No. 6, 991 (1981).

46. H. Hurwitz and R. C. Jones, *J. Opt. Soc. Am.*, **31**, No. 7, 493 (1941).

47. R. C. Jones, *J. Opt. Soc. Am.*, **31**, No. 7, 488 (1941).

48. R. M. A. Azzam and N. M. Bashara, *Ellipsometry and Polarized Light*, North-Holland, Amsterdam (1977), p. 529.

49. A. M. Sergeev, V. M. Gelikonov, G. V. Gelikonov, et al., *Opt. Express*, **1**, No. 13, 432 (1997).